

Post-Test Analysis of the Deep Space One Spare Flight Thruster Ion Optics

John R. Anderson, Anita Sengupta, John R. Brophy

*Jet Propulsion Laboratory
California Institute of Technology
Pasadena, California*

The Deep Space 1 (DS1) spare flight thruster (FT2) was operated for 30,352 hours during the extended life test (ELT). The test was performed to validate the service life of the thruster, study known and identify unknown life limiting modes. Several of the known life limiting modes involve the ion optics system. These include loss of structural integrity for either the screen grid or accelerator grid due to sputter erosion from energetic ions striking the grid, sputter erosion enlargement of the accelerator grid apertures to the point where the accelerator grid power supply can no longer prevent electron backstreaming, unclearable shorting between the grids caused by flakes of sputtered material, and rouge hole formation due to flakes of material defocusing the ion beam. Grid gap decrease, which increases the probability of electron backstreaming and of arcing between the grids, was identified as an additional life limiting mechanism after the test. A combination of accelerator grid aperture enlargement and grid gap decrease resulted in the inability to prevent electron backstreaming at full power at 26,000 hours of the ELT. Through pits had eroded through the accelerator grid webbing and grooves had penetrated through 45% of the grid thickness in the center of the grid. The upstream surface of the screen grid eroded in a chamfered pattern around the holes in the central portion of the grid. Sputter deposited material, from the accelerator grid, adhered to the downstream surface of the screen grid and did not spall to form flakes. Although a small amount of sputter deposited material protruded into the screen grid apertures, no rouge holes were found after the ELT.

Introduction

The Deep Space One (DS1) spacecraft--launched on October 24, 1998--used a 30-cm-diameter NASA Solar electric propulsion Technology Application Readiness (NSTAR) xenon ion thruster as its primary propulsion system. DS1 was a technology validation mission and successfully completed its mission to

flyby Asteroid Braille and Comet Borelly. When the mission ended in December 2001, the ion thruster had processed over 73 kg of propellant and had accumulated 16,265 hours of operation in space. Details on the DS1 ion thruster performance can be found in references [1-3]. The mission was a success, stimulating future NASA science missions utilizing solar electric propulsion to demand lifetimes and propellant throughput in excess of 20,000 hours and 200 kg. As a result, assessing the ultimate service life capability of the technology is vital, requiring extensive ground testing and analysis.

Prior to the DS1 mission, an extensive testing program was conducted including several endurance tests performed on engineering model thrusters. These tests were conducted to flight qualify the ion thruster technology by characterizing engine

Copyright Statement

performance, understanding the interaction of the thruster plume with the spacecraft, and identifying dominant engine life limiting modes. The long duration tests were used to identify unexpected life limiting modes, and to characterize the parameters that drive potential life limiting modes and engine performance degradation. The program included a 2,000 hour test, 1,000 hour test and the 8,000 hour test Life Demonstration Test (LDT), all with engine operation at full power. Several potential life limiting mechanisms were identified as a result of these tests, and modifications were made to the flight engine design. Details of these previous endurance tests including life limiting mode analysis and suggested design modifications can be found in references [4-7]. Two flight thrusters, designated FT1 and FT2, were fabricated for the DS1 mission [8]. FT1 was integrated onto the spacecraft and FT2 was designated the flight spare thruster. Prior to the launch of DS1, an extended life test (ELT) of the flight spare ion thruster began on October 05, 1998 at Jet Propulsion Laboratory. The thruster was under vacuum throughout the test which was voluntarily terminated on June 26, 2003. During this world record breaking test the thruster was operated for 30,352 hours and processed 235 kg of xenon propellant.

Prior to the LDT, seven possible credible life limiting modes for the NSTAR ion engine [9] were identified. Of these, five are related to the ion optics system, the subject of this paper. One mode is shorting of the screen and accelerator grids with flakes of conductive material. Another mode is flakes defocusing the ion beam resulting in direct ion impingement on the accelerator grid leading to accelerator grid loss of structural integrity or electron backstreaming. Two additional modes are loss of structural integrity of the screen or accelerator grid caused by discharge chamber ion impingement on the screen grid or sputter induced erosion of the accelerator grid due to charge exchange ion impingement. The fifth life limiting mode is electron backstreaming due to accelerator grid hole enlargement. As a result of the NSTAR thruster testing, grid gap decrease was identified as a new mechanism that shortens thruster life by decreasing the ability to prevent electron backstreaming.

The purpose of this paper is to present preliminary results of the on-going post test analysis of the ion optics system from the ELT. The ion optics system is designed to electrostatically accelerate propellant ions from the discharge chamber into a high velocity beam, thereby producing thrust. The NSTAR ion optics system has closely spaced screen and accelerator grids with thousands of aligned matching

apertures. The screen grid is biased between 650 and 1,100 V while the accelerator grid is biased between -150 and -250 V. A brief discussion of the relationship between the ion optics and the life limiting modes is given prior to presenting results.

Life Limiting Modes

Grid Short

The ion optics can be shorted by conductive debris that becomes lodged between the screen and accelerator grids. Potential sources for this debris include material from the launch environment, material left over from the thruster fabrication, and flakes formed when thin films of sputter deposited material spall off of the surface of an ion engine component. A short caused by debris from the launch environment is suspected as the cause of the continuous recycling that resulted in the DS1 thruster shutdown 4.5 minutes after its first start in space [1]. In another case, failure to clear a grid-to-grid short caused termination of an accelerated wear test of a two-grid ion optics system [10].

Flakes are more likely to be a problem late in thruster life because they are formed from thin films of sputter deposited material that accumulate during thruster operation. The accelerator grid, which is subjected to bombardment by high energy charge-exchange ions, is a source of sputtered material. Sputtered material from the accelerator grid holes is deposited on the screen grid and some finds its way through the screen grid apertures and deposits on discharge chamber surfaces. Although less severe than accelerator grid erosion, material is also sputtered from the upstream surface of the screen grid. In the ELT significant erosion of the discharge cathode assembly was also observed [11] and this is a non-negligible source of material. Deposited material can spall off of surfaces due to mechanical stressing brought on by changes in temperature caused by changes in thruster operating conditions.

The DS1 ion propulsion system was designed with a system that can be used to try to clear these shorts by driving a 4 A current through the short. Details of this system are described in Reference [12].

Rouge Holes

Flakes, or accumulated sputter deposited material, can also cause defocusing of ion beamlets if they become lodged on the screen grid. Such material can steer a portion of the ion beamlet directly onto the accelerator grid. The high energy ions directly impinging on the accelerator grid cause rapid erosion

of the grid, which can lead to accelerator grid loss of structural integrity or electron backstreaming. Accumulated sputter deposited material extending about 200 μm into screen grid holes is thought to have caused deflection of ions onto the accelerator grid resulting in damage observed at 5 locations during the accelerated wear test described in Reference [10].

Methods to mitigate problems associated with flakes have been developed [13]. Adhesion of sputtered films is enhanced when the surface has been roughened or films are deposited on a fine wire mesh. If the material does spall from the wire mesh, the flake size is on the order of the mesh diameter. The NSTAR ion thruster has a fine wire mesh installed in the discharge chamber, but not on the grids. Neither the NSTAR thruster screen or accelerator grid surfaces were roughened prior to the ELT. Although there was no evidence of flakes spalling from the screen grid, flakes were found in the discharge chamber after the ELT; these flakes are believed to be a test facility effect and are described in detail in Reference [14].

Screen Grid Loss of Structural Integrity

Discharge chamber ions that strike the screen grid webbing cause erosion that can eventually result in grid loss of structural integrity. The ions tend to chamfer the edge of the upstream holes of the screen grid. The erosion rate is dependent on the energy of the ions striking the grid and the fraction of doubly-charged ions; the energy of singly-charged ions in eV is approximately equal to the discharge voltage in volts, while the doubly-charged ions have twice the energy of the singly-charged ions. At typical discharge chamber voltages the erosion rate increases rapidly with energy [15], so it is desirable to operate at as low a discharge voltage as practical.

Accelerator Grid Loss of Structural Integrity

Charge-exchange ions impinging on the downstream surface of the accelerator grid causes a "pits and grooves" erosion pattern. The pits and grooves typically form in the center of the webbing leaving a relatively uneroded portion of webbing near the holes. The pits and grooves can eventually penetrate through the entire webbing thickness resulting in accelerator grid loss of structural integrity. If this occurs, a section of webbing detaches from the grid. This section of material could short the screen and accelerator grids. If the section of webbing falls away from the accelerator grid it would leave a large

enough open area that electron backstreaming could no longer be prevented.

Electron Backstreaming

Electron backstreaming occurs when the potential at the center of the accelerator grid aperture is not sufficiently negative to prevent charge neutralizing electrons in the ion beam downstream of the thruster from flowing upstream into the discharge chamber. Backstreaming electrons do not produce thrust and the energy they gain while traveling into the discharge chamber is dissipated as heat in the discharge chamber. Each backstreaming electron consumes the same amount of energy that accelerating a thrust producing beam ion does; because electrons are more mobile than ions much larger electron currents could backstream resulting in little or no thrust and overheating of the discharge chamber. Therefore the thruster must be operated in such a way that electron backstreaming is prevented at all times.

In practice the potential at the center of the aperture is kept sufficiently negative to prevent electron backstreaming by biasing the accelerator grid a few hundred volts negative. The magnitude of the accelerator grid voltage required to prevent electron backstreaming depends on several factors including the electric field between the grids, the accelerator aperture diameter and the beam current density. Charge exchange ions erode the barrel of the accelerator grid holes causing them to enlarge. As the holes enlarge the negative grid surface moves further from the center of the hole, requiring more negative accelerator grid voltages to prevent electron backstreaming. The ion propulsion system fails when the magnitude of the potential required to prevent electron backstreaming exceeds the voltage capabilities of the accelerator grid bias supply.

The inability to prevent electron backstreaming at full power was the first life limiting mode encountered during the ELT. The thruster could still be operated at less than full power and additional operation at reduced power was conducted prior to terminating the test.

Grid Gap Decrease

In addition to the previously identified life limiting modes a new potential life limiting mechanism was identified as a result of post-test ion optics measurements. Post-test examination of the ion optics assembly revealed that the cold gap between the screen and accelerator grids had decreased significantly (~30%) during the ELT. A decrease in the cold grid gap (~12%) was also observed after the

LDT. This grid gap decrease increases the electric field between the grids and results in increased susceptibility to electron backstreaming and arcing between the grids. A combination of grid gap decrease and accelerator aperture enlargement resulted in the electron backstreaming failure at full power experienced during the ELT.

Ion Optics System

The two-grid ion optics system for the NSTAR thruster [16] has a 3.81×10^{-4} m (nominal) thick screen grid and a 5.08×10^{-4} m (nominal) thick accelerator grid. The initial screen grid hole diameter was 1.91×10^{-4} m and the initial accelerator grid hole diameter was 1.14×10^{-4} m. The holes were arranged in a hexagonal close pack pattern with a hole-to-hole spacing of 2.22×10^{-3} m, resulting in initial physical open area fractions of 0.67 and 0.24 for the screen and accelerator grids, respectively. The nominal cold gap between the molybdenum grids is 6.6×10^{-4} m. The grids are dished outward to form a spherical segment with a nominal spherical radius of 0.5 m. Each of the electrodes is riveted to a molybdenum stiffening ring. The grids are attached to a titanium mounting structure which is attached to the discharge chamber.

The FT2 optics system was tested for 30,352 hours during the ELT. Subsequent to the test the ion optics were removed from the thruster and the screen and accelerator grid were weighed. The post test mass of the accelerator and screen grids were 577.0 and 439.9 grams, respectively. The pre-test mass of the accelerator and screen grids were 610.7 and 443.1 grams, respectively. The accelerator grid lost 33.7 grams of material and the screen grid lost 3.2 grams of material. The accelerator grid had molybdenum eroded from the pits and grooves pattern as well as the aperture walls. In addition, the accelerator had backsputtered carbon build up on the outer edge of the grid as well as in a scallop pattern around each of the holes. The estimated mass of backsputtered carbon is 0.6 grams, which would give a total accelerator grid molybdenum mass loss of 33.1 grams.

Screen Grid Results

Post-test analysis of the screen grid includes profilometry measurements of the erosion on the upstream surface, photography to document the grid condition and estimate the size and extent of accumulated material protruding into the apertures, and measurement of the aperture diameters. Sectioning of the screen grid so that the thickness of

sputter deposited material on the downstream surface can be measured is planned.

Post-test profilometry was obtained on the upstream surface of the screen grid at various locations. Shown in Figure 1 is a profilometry scan taken at the center of the screen grid. Chamfering of the upstream surface is evident; the highest points are located on the webbing at the symmetry points furthest from the three surrounding holes. Figure 2 is a two-dimensional plot of the data shown in Figure 1. Also shown in Figure 2 are lines representing cross-sections across the webbing. The path labeled A-A is a typical cut across the thin section of the webbing and is located at the 4 o'clock position in the plot; there are a total of 6 of these cross-sections shown in Figure 2. The path labeled B-B cuts through the high points and along the ridge line of the chamfer pattern. Figure 3 shows the six cuts across the thin part of the webbing (including path labeled A-A). The erosion around the center hole is nearly uniform. The difference in elevation between the ridge and the edge of the webbing is about ~ 25 μm .

Figure 4 show the cross-section along path B-B which traverses the ridge line between two high points. The ridge drops is about ~ 25 μm between the peaks. The most severe chamfering occurs between the peaks and the hole where the height decreases about ~ 60 μm .

Measurements of the screen grid thickness indicate the maximum thickness is the same as the manufactured thickness of 3.8×10^{-4} m. Typically sputtered material from the accelerator grid deposits on the downstream side of the screen grid. After the LDT the sputter deposited layer was ~ 10 μm thick; because the ELT ran longer than the LDT it is anticipated that thicker layers of sputter deposited material will be found when the screen grid is sectioned and these measurements are made. The peaks on upstream surface of the screen grid may have receded due to erosion; however, the sputter deposited material on the downstream surface equaled the amount of material removed from the upstream surface resulting in the same pre- and post-test grid thickness. Each hole in the screen grid has a hexagonal area associated with it; the perimeter of this area is made up of the ridge lines running between the 6 peaks surrounding a hole. The net mass loss per hole was estimated by integrating the profilometry data over the upstream surface to determine the volume of the remaining material and multiplying by the mass density of molybdenum. The mass loss data for the screen grid is shown in Figure 5. Profilometry of the screen grid was obtained out to 5 cm radius on the thruster. At the

center hole the mass loss was 0.96 mg/hole which is 17% of the initial mass of webbing surrounding the hole. Although profilometry was only obtained out to 4.5 cm thruster radius photographs show that chamfering diminishes at larger thruster radii and is almost non-existent at thruster radii greater than 8.5 cm.

Although more data will be obtained to provide information on the radial mass loss variation across the grid, the existing data along with limiting case assumptions can be used to provide minimum and maximum estimates of the net mass loss by integrating over the local mass loss data. If it is assumed that the mass loss per hole decreases to zero at 8.5 cm, the integrated net mass loss is 2.2 g. If it is assumed that the mass loss per hole is constant between 4.5 cm and 8.5 cm at the 4.5 cm radius value, the integrated net mass loss is 4.0 g. The values of 2.2 and 4.0 g are observed to bracket the measured mass loss of 3.2 g.

Figure 6 shows a view of the upstream side of the screen grid webbing near the center of the grid. Evident in the photo is the chamfering of the upstream side of the grid as well as rough edges along the apertures. The material protruding into the apertures is sputtered material that deposited on the downstream side of the screen grid cusp. The largest protrusion extends about 40 μm into the aperture. Since no rouge holes were observed after the conclusion of the ELT, this protrusion did not cause enough beamlet distortion to result in damage such as that observed in Ref [10]. Figure 7 shows additional photographs of the upstream side of the screen grid at locations where profilometry was obtained. In the ELT screen grid these protrusions are evident in the photographs at thruster radius out to 2.3 cm and are not discernable in the photographs at and beyond 3.4 cm thruster radius.

Figure 8 shows post-test screen grid aperture diameters measured with an optical CMM. The nominal manufactured aperture diameter is shown for reference; measured pre-test aperture diameters were within 0.01 mm of the nominal dimension. The data in Figure 8 suggest that the screen grid hole diameters decreased slightly less than 1% due to sputter deposited material accumulating on the downstream side of the grid.

Accelerator Grid Results

Post-test analysis of the accelerator grid includes profilometry to measure the wear in the pits and grooves pattern, photography to document the condition of the grid, and measurement of the aperture diameters. Sectioning of the accelerator grid

to obtain cross-section profiles through the pits and grooves pattern, the bridge pattern and the aperture wall eroded pattern is planned.

After the conclusion of the ELT profilometry data was obtained at a number of locations on the accelerator grid. Figure 9 shows a three-dimensional view of profilometry data taken on the downstream side of the accelerator grid at a location near the center of the grid. The pits and grooves pattern on the webbing between the apertures is clearly visible. Figure 10 a two-dimensional plot of the same data. Also shown in Figure 10 are lines cutting through cross-sections of the bridge pattern (section A-A) and through the pits and grooves pattern (section B-B).

The cross-section through the pits and grooves pattern near the center of the grid is shown in Figure 11. The cross-section cuts through two holes, the pits centered in the regions of the webbing furthest from the three holes surrounding each pit, and through the groove between two pits. During the ELT the pits wore completely through the grid inside a thruster radius of 5.6 cm. The grooves in the vicinity of the center hole eroded to a depth of 230 μm or about 45% of the thickness of the grid.

To determine if there were variations in the groove depth around the center hole, cross-sections of the profilometry data along the five lines cutting through the grooves shown in Figure 10 (section A-A) were obtained. These cross-sectional data are shown in Figure 12. The erosion pattern appears to be uniform around the center aperture. All 5 cross-sections are similar and the depth of the groove is about 230 μm .

When the groove erodes through the webbing the accelerator grid structurally fails. Once through pits occur, ions travel through the holes and are reflected back onto the upstream side of the accelerator grid. These reflected ions begin to undercut the upstream side of the grid, hastening loss of structural integrity. This undercutting is evident in Figure 13, which shows the upstream side of the accelerator grid near the center of the grid. The triangular through pit is surrounded by an oval shaped region which has been undercut to a depth of 65 μm . It is estimated that the accelerator grid lost 0.3 g of mass in the undercuts.

Pits and grooves cross-sections from the center out to 9.5 cm thruster radius are shown in Figure 14. The eroded depth in the groove region is nearly uniform out to a radius of 4.5 cm. The depth decreases slightly between 4.5 cm and 8.6 cm. Between 8.6 and 9.5 cm the eroded depth decreases to almost zero, indicating that the beam current density is significantly lower at thruster radii greater than 9.5 cm than it is in the central portion of the thruster.

The downstream accelerator grid profilometry data was integrated to determine the volume remaining in the webbing. This was subtracted from the initial (uneroded) webbing volume and the difference multiplied by the mass density of the grid material to determine the mass loss in the pits and grooves pattern. Figure 15 shows integrated mass loss per hole in the pits and grooves pattern. Each pit is split between 3 holes and each groove between 2 holes. Since there are 6 pits and 6 grooves surrounding each hole, there are two pits and three grooves associated with each hole. The mass loss per hole is ~3.5 mg/hole near the center of the grid and decreases to about 2.8 mg/hole at about 8.6 cm. The grid transitions from net erosion to net carbon deposition between about 8.6 cm and 9.5 cm. The mass loss data was integrated over the grid yielding an estimate of 17.3 g mass loss in the pits and grooves pattern.

Accelerator grid aperture diameters measured after the ELT and LDT are shown in Figure 16. The post-test ELT data in Figure 16 were taken across the grid at three different azimuthal locations. The differences in the data indicate that the wear pattern is azimuthally asymmetric.

The diameters shown are the minimum aperture diameter. Photographs of the grids suggest that the apertures were chamfered toward the downstream surface after the ELT. Although better measurements of the eroded aperture cross-sections will be made after the grids are sectioned, it is estimated from the photographs that the downstream screen diameter is ~15% larger than the upstream diameter for thruster radii less than about 8.6 cm. Using this estimate and averaging the aperture diameters shown in Figure 16, the mass loss per hole due to aperture wall erosion, shown in Figure 17, was estimated. It is estimated that 2.7 mg per hole is lost near the center of the thruster and the mass loss per hole decreases to almost zero at large thruster radii. Cross over ions resulting from poor focusing, due to low plasma density, results in erosion of near the edge of the grids; this causes the increase in mass loss per hole at the outer edge of the grid. Integrating the mass loss per hole over the grid yields an estimate of 12.2 g lost due to aperture wall erosion.

Integrating the local mass loss estimates for pits and grooves erosion, aperture wall erosion and undercutting over the grid and summing the result yields an estimated mass loss of 29.8 g for the accelerator grid. To obtain an estimate of the mass change for the accelerator grid over the course of the ELT, the carbon deposition must be subtracted from this; it is estimated that between 0.5 and 0.8 g of sputter deposited carbon accumulated on the grid. This gives a mass change estimate which is ~15%

lower than the measured mass difference of 33.7 g. As noted earlier, better estimates of the local mass loss will be obtained when the grids are sectioned and the shape of the erode apertures is determined. The sectioned grids should also provide additional data on the azimuthal variation in grid wear.

ELT Pits Erosion Data

In addition to the post-test profilometry data, profilometry was also obtained during the ELT. Profilometry of selected regions of the accelerator grid were obtained at intervals of 1,000 to 2,000 hours using a DynaVision LTS 15/2.9 Laser Sensor. Pit depth data as a function of run time is shown in Figure 18, which shows data for the first 10,451 hours of the test. Although data was collected after 10,451 hours, multiple reflections of the laser light from the walls of the pits caused problems with obtaining good depth readings once the pit depth exceeded about half the accelerator grid thickness. During the first 10,451 hours of the ELT the thruster was operated at three different throttle levels. For the first 448 hours, the thruster was operated at 1.96 kW; then the throttle level was changed to 2.3 kW (full power) until 4,937 hours; when the thruster was throttled to 1.46 kW.

Profilometry was performed on the webbing adjacent to the center hole and along a radius at 2.9, 5.7 and 8.6 cm from the center of the grid. The pit depth at the center hole at the conclusion of the full power segment was 170 μm ; the pit depth at the center of the accelerator grid during the LDT, which was run at full power, was about 155 μm at the same run time [17]. During both the ELT and the LDT initial erosion rate over the first ~2,000 hours was about 45 $\mu\text{m}/\text{hr}$. After ~2,000 hours the center hole pit erosion rate decreased to an approximately constant rate of 25 $\mu\text{m}/\text{hr}$. In the ELT after ~2,000 hours the center aperture pit erosion rate was 23 $\mu\text{m}/\text{hr}$ until the throttle level was changed at 4,937 hours. During the ELT 1.46 kW test segment, the center hole pit erosion rate was 13 $\mu\text{m}/\text{hr}$.

Grid Gap Change (Structural Analysis)

As noted earlier the gap between the screen and accelerator grids decreased during both the ELT and the LDT. The pre- and post-test grid gap data are shown in Figure 19. The cold grid gap changed from the nominal value of 660 μm prior to the test to a post-test gap of 460 μm ; this change in gap contributed to the thruster electron backstreaming limit being exceeded at full power during the ELT.

In order to determine what caused the grid gap change, a preliminary structural analysis of the ion optics system was performed. The finite element model used in the analysis is shown in Figure 20. Shown are the accelerator grid stiffening ring mounted on top the optics ring which attaches to the thruster. The accelerator grid electrode, which attaches to the stiffening ring, was modeled analytically and is not shown in the finite element model drawing. Residual stresses from the manufacture of the electrode were determined and applied to the stiffening ring. During thruster operation at normal optics temperatures (~200 C) the residual stresses in the electrode transmit forces to the stiffening ring which result in a stress level of ~75 ksi in the stiffening ring. The stress levels in the stiffening ring are shown in Figure 21. The yield strength for the molybdenum stiffening ring is 80 ksi at room temperature but the yield strength decreases to about 63 ksi at 200 C; as a result permanent deformation of the stiffening ring tabs is expected. Under these conditions the prediction from the analysis is that the grid gap will decrease to 400 μm .

In the preliminary structural analysis, it was assumed that the accelerator grid electrode did not exceed its yield strength; however, the post-test measurement show that both the electrode and the stiffening ring deformed. The accelerator grid electrode is domed with a flat area at the outer edge which is riveted to the stiffening ring. After the ELT the stiffening ring was detached from the electrode. The outer edge of the stiffening ring tabs, which was designed to be flat, were deflected up an average of 50 μm . The outer edge of the electrode, which also was designed to be flat, had deflected upward by an average of 210 μm . Although the accelerator grid electrode needs to be modeled more accurately, the conclusion from the structural analysis is that the grid gap change is caused by residual stresses introduced during the manufacturing of the grids. In order to correct this problem, the electrode should be stress relieved or the optics assembly should be redesigned to accommodate the manufacturing stresses.

Conclusions

After 30,352 hours of operation and processing 235 kg of propellant, the NSTAR ion thruster was still functioning when the extended life test was voluntarily terminated. The first life limiting mode encountered during the test was inability to prevent electron backstreaming at full power; although the thruster could not be operated at full power, it could

still operate at reduced power levels where the beam current density was lower. The accelerator grid did not suffer loss of structural integrity during the test; however, through pits had eroded through the webbing in the central portion of the grid. The upstream surface of the screen grid eroded in a chamfered pattern, while sputter deposited material from the accelerator grid accumulated on the downstream surface, resulting in a net loss of 17% of the mass near the center of the grid. None of the material sputter deposited on the screen grid spalled to produce flakes. Although a small amount of sputter deposited material protruded into the screen grid apertures, no rouge holes were found after the ELT. Deformation of the accelerator grid electrode and stiffening ring caused the cold grid gap to decrease, which contributed to the inability to prevent electron backstreaming during the ELT.

Acknowledgements

The research described in this paper was carried out by the Jet Propulsion Laboratory, California Institute of Technology, under a contract with the National Aeronautics and Space Administration.

References

1. Polk, J. E., Brinza, D., Kakuda, R. Y., Brophy, J. R., Katz, I., Anderson, J. R., Rawlin, V. K., Patterson, M. J., Sovey, J., Hamley, J., "Demonstration of the NSTAR Ion Propulsion System on the Deep Space One Mission," IEPC-2001-075, 27th International Electric Propulsion Conference, Pasadena, CA, October 2001.
2. Polk, J. E., Kakuda, R. Y., Anderson, J. R., Brophy, J. R., Rawlin, V. K., Patterson, M. J., Sovey, J., Hamley, J., "Validation of the NSTAR Ion Propulsion System on the Deep Space One Mission: Overview and Initial Results," AIAA-99-2274, 35th AIAA/ASME/SAE/ASEE Joint Propulsion Conference and Exhibit, Los Angeles, CA, June 1999.
3. Polk, J. E., Kakuda, R. Y., Anderson, J. R., Brophy, J. R., Rawlin, V. K., Sovey, J., Hamley, J., "In-Flight Performance of the NSTAR Ion Propulsion System on the Deep Space One Mission," IEEE-8.304, IEEE 2000 Aerospace Conference Proceedings, Big Sky, MT, March 2000.
4. Patterson, M. J., Rawlin, V. K., Sovey, J. S., Kussmaul, M. J., Parkes, J., "2.3 kW Ion

- Thruster Wear Test," AIAA-95-2516, 31st AIAA/ASME/SAE/ASEE Joint Propulsion Conference and Exhibit, San Diego, CA, July 1995.
5. Polk, J. E., Patterson, M. J., Brophy, J. R., Rawlin, V. K., Sovey, J. S., Myers, R. M., Blandino, J. J., Goodfellow, K. D., Garner, C. E., "A 1000 Hour Wear Test of NASA's NSTAR Ion Thruster," AIAA-96-2784, 32nd AIAA/ASME/SAE/ASEE Joint Propulsion Conference and Exhibit, Lake Buena Vista, FL, July 1996.
 6. Polk, J. E., Anderson, J. R., Brophy, J. R., "Behavior of the Thrust Vector in the NSTAR Ion Thruster," AIAA-98-3940, 34th AIAA/ASME/SAE/ASEE Joint Propulsion Conference and Exhibit, Cleveland, OH, July 1998.
 7. Polk, J. E., Anderson, J. R., Brophy, J. R., Rawlin, V. K., Patterson, M. J., Sovey, J., Hamley, J., "An Overview of the Results from an 8200 Hour Wear Test of the NSTAR Ion Thruster," AIAA-99-2446, 35th AIAA/ASME/SAE/ASEE Joint Propulsion Conference and Exhibit, Los Angeles, CA, June 1999.
 8. Christensen, J., Freick, K. J., Hamel, D. J., Hart, S. L., Norenberg, K. T., Haag, T. W., Patterson, M. J., Rawlin, V. K., Sovey, J. S., Anderson, J. R., Becker, R. A., Polk, J. E., "Design and Fabrication of a Flight Model 2.3 kW Ion Thruster for the Deep Space 1 Mission," AIAA-98-3327, 34th AIAA/ASME/SAE/ASEE Joint Propulsion Conference and Exhibit, Cleveland, OH, July 1998.
 9. Brophy, J. R., Polk, J. E. and Rawlin, V. K., "Ion Engine Service Life Validation by Analysis and Testing," AIAA-96-2715, 32nd AIAA/ASME/SAE/ASEE Joint Propulsion Conference and Exhibit, Lake Buena Vista, FL, July 1996.
 10. Brophy, J. R., Polk, J. E., and Pless, L. C., "Test-to-failure of a Two-Grid, 30-cm-dia. Ion Accelerator System," IEPC-93-172, 23rd International Electric Propulsion Conference, Seattle, WA, Sept. 1993.
 11. Sengupta, A., Brophy, J. R., Goodfellow, K. D., "Status of the Extended Life Test of the Deep Space 1 Flight Spare Ion Engine after 30,352 Hours of Operation," AIAA-2003-4558, 39th AIAA/ASME/SAE/ASEE Joint Propulsion Conference and Exhibit, Huntsville, AL, July 2003.
 12. Goodfellow, K. D., Ganapathi, G. B., Stocky, J. F., "An Experimental and Theoretical Analysis of the Grid Clearing Capability of the NSTAR Ion Propulsion System," AIAA-99-2859, 35th AIAA/ASME/SAE/ASEE Joint Propulsion Conference and Exhibit, Los Angeles, CA, June 1999.
 13. Powers, J. L., Hiznay, D. J., "Solutions for Discharge Chamber Sputtering and Anode Deposit Spalling in Small Mercury Ion Thrusters," NASA TM X-71675, March, 1975.
 14. de Groh, K. K., Banks, B.A., Karniotis, C. A., "NSTAR Extended Life Test Discharge Chamber Flake Analyses," AIAA-2004-3612, 40th AIAA/ASME/SAE/ASEE Joint Propulsion Conference and Exhibit, Fort Lauderdale, FL, July, 2004.
 15. Doerner, R. P., Whyte, D. G., Goebel, D. M., "Sputtering yield measurements during low energy xenon plasma bombardment," *Journal of Applied Physics*, Vol. 93, No. 9, pp. 5816-5823, 1 May 2003.
 16. Patterson, M. J., Rawlin, V. K., Sovey, J. S., Kussmaul, M. J., Parkes, J., "2.3 kW Ion Thruster Wear Test," NASA TM 107076, July, 1995.
 17. Polk, J. E., Anderson, J. R., Brophy, J. R., Rawlin, V. K., Patterson, M. J., Sovey, J., "In Situ, Time-Resolved Accelerator Grid Erosion Measurements in the NSTAR 8000 Hour Ion Engine Wear Test," IEPC-97-047, 25th International Electric Propulsion Conference, Cleveland, OH, August 1997.

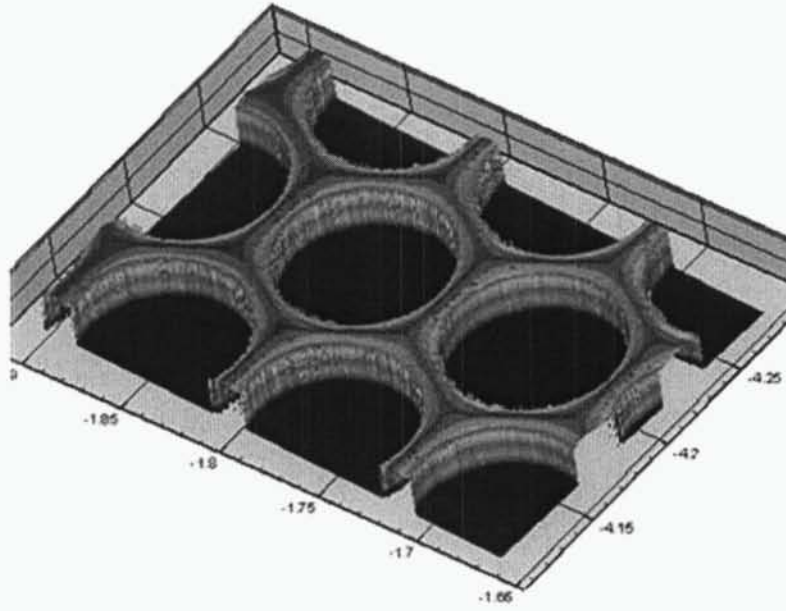


Figure 1. Upstream Screen Grid Profilometry at Center Hole

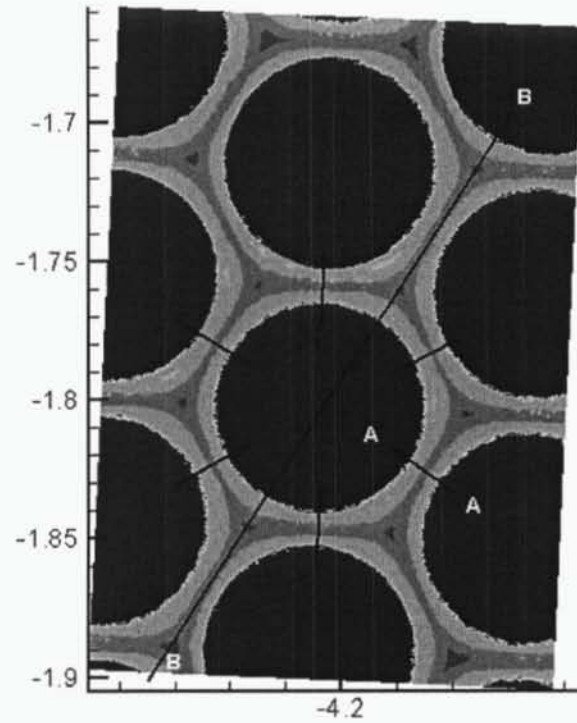


Figure 2. Upstream Screen Grid Profilometry at Center Hole

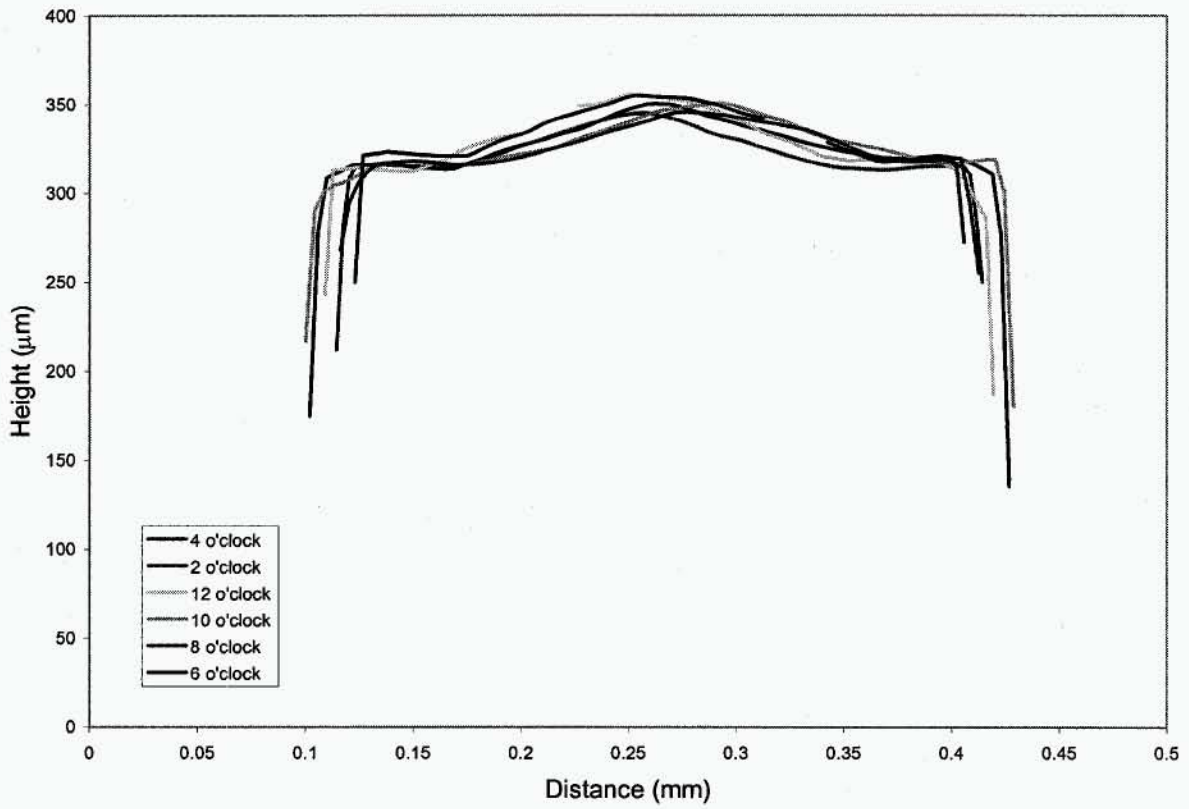


Figure 3. Upstream Screen Grid Surface Cut Along Paths A-A

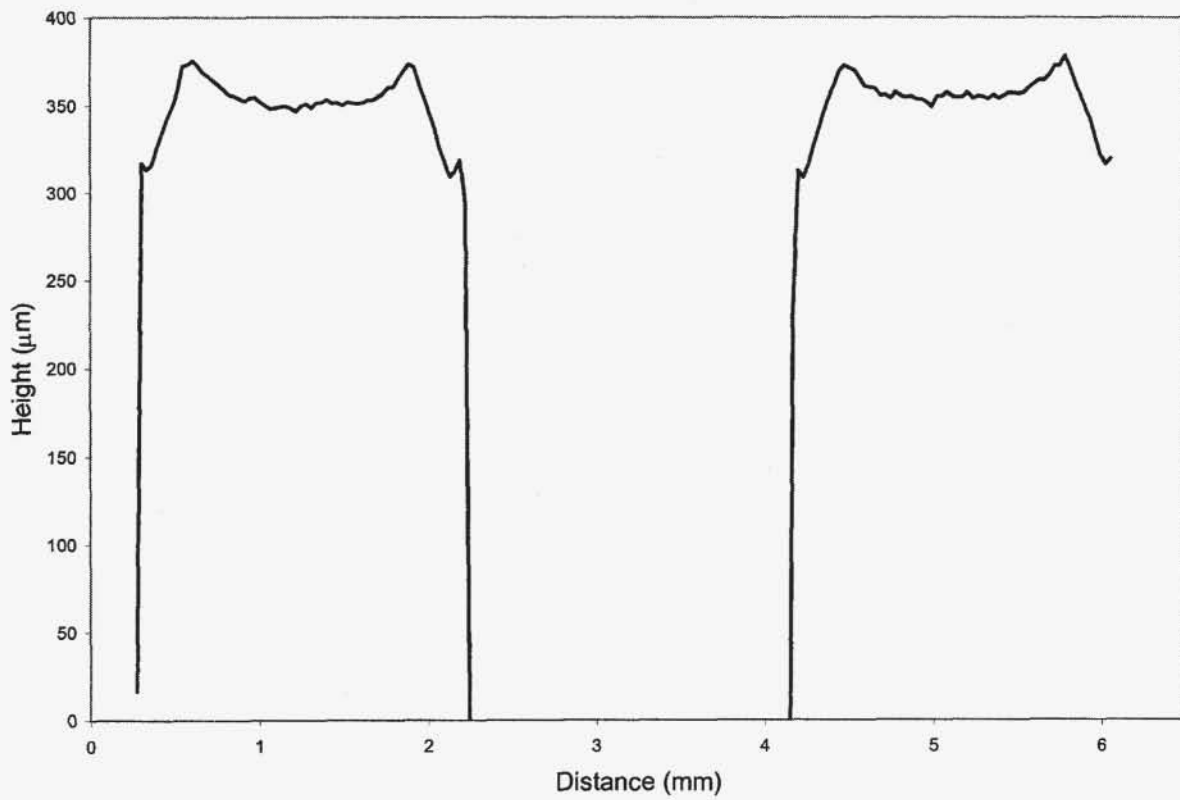


Figure 4. Upstream Screen Grid Profilometry Cut Along Path B-B

Net Mass Loss Per Screen Hole

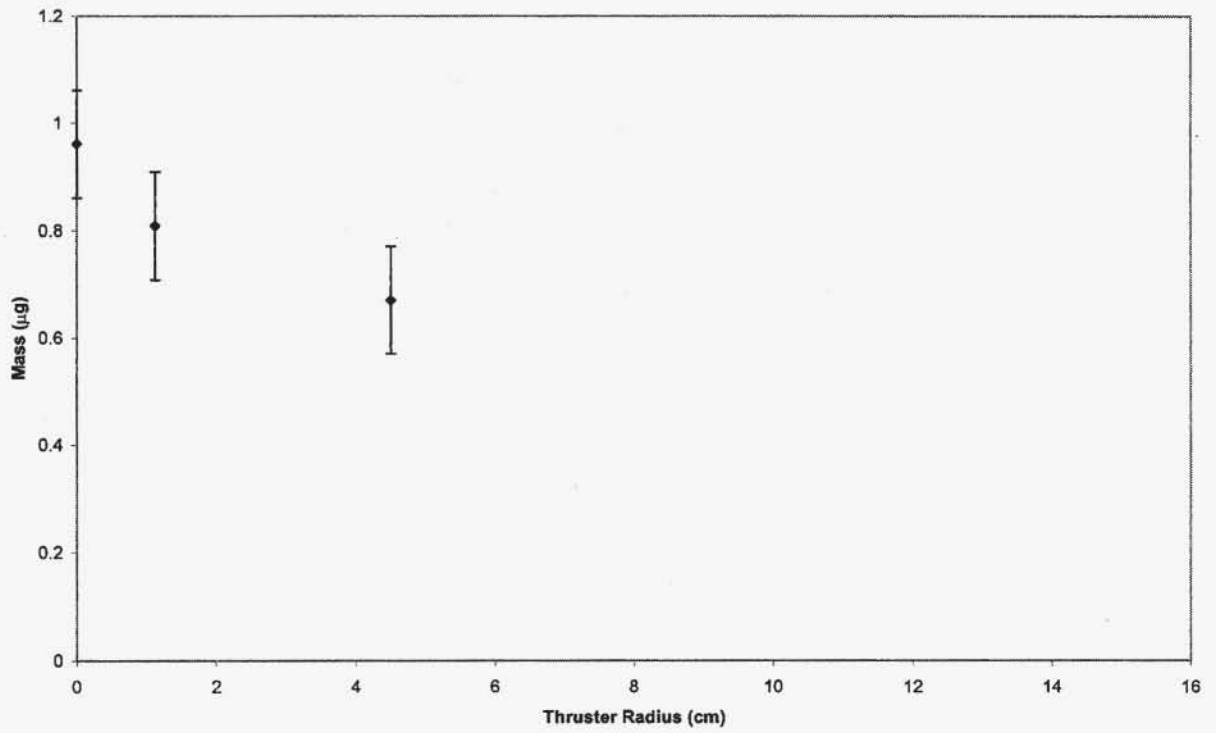


Figure 5. Screen Grid Net Mass Loss per Hole

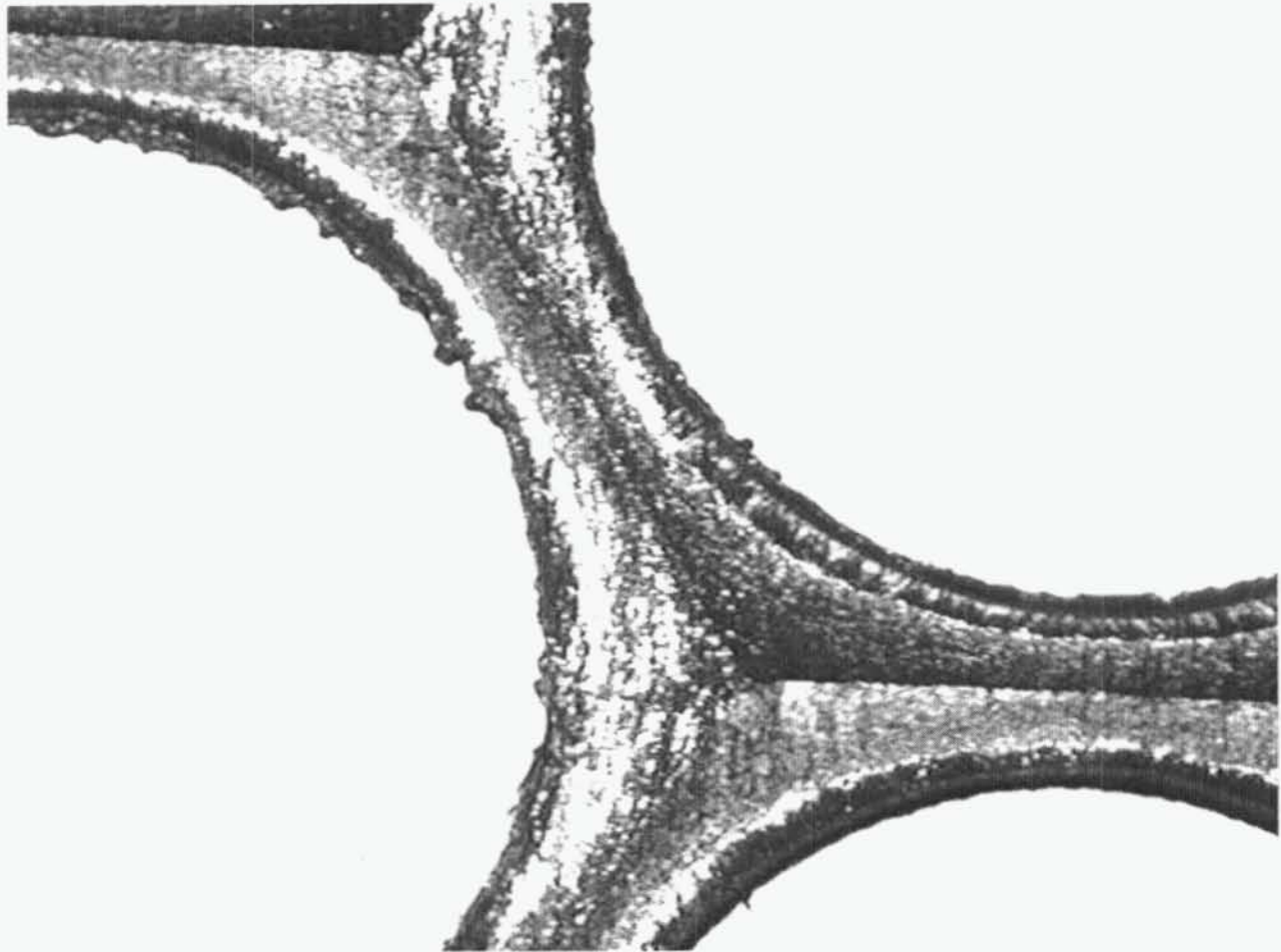


Figure 6. Screen Grid Webbing Near Center Hole Viewed From the Upstream Side

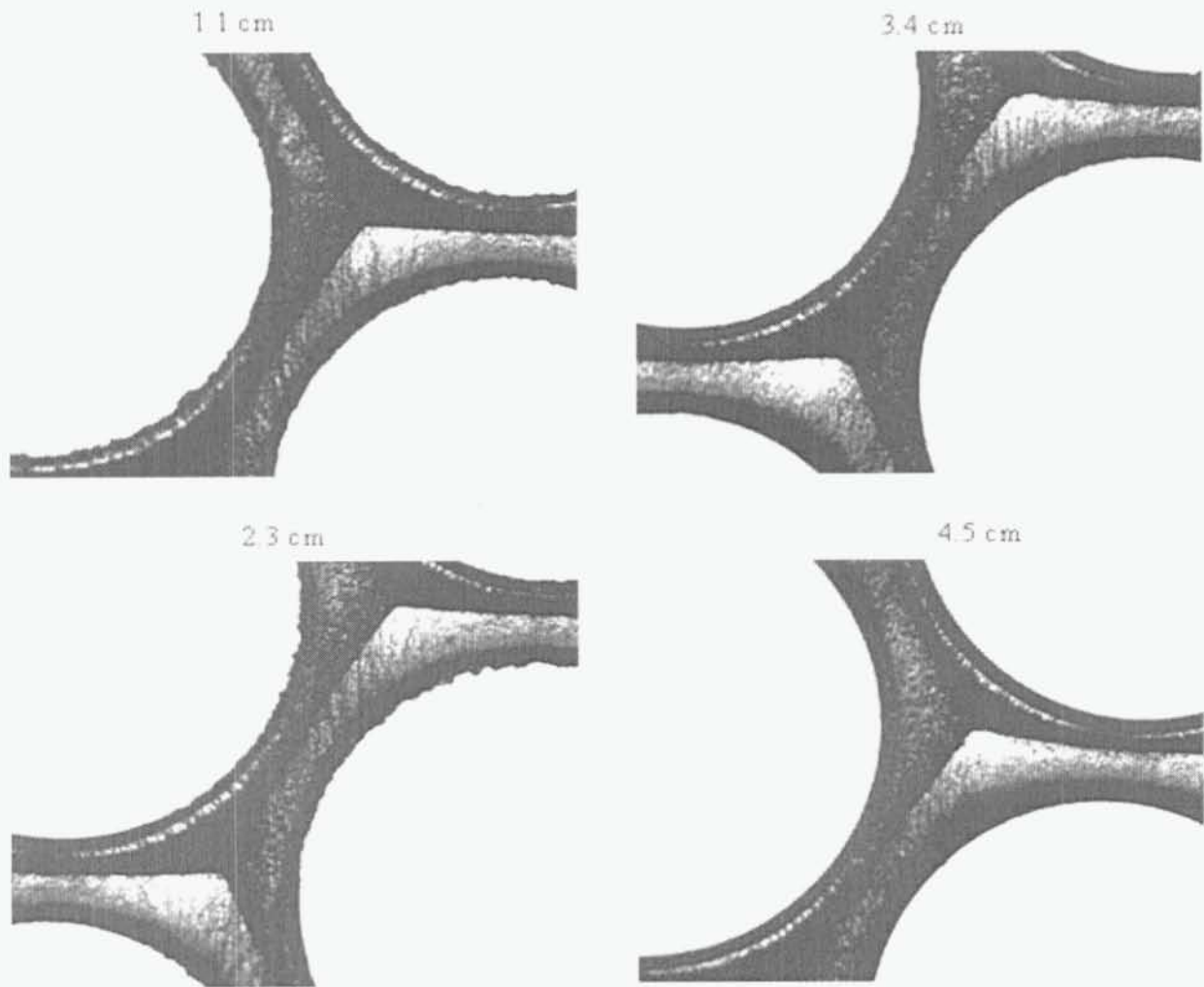


Figure 7. Screen Grid Webbing at Locations Where Profilometry was Obtained

Post-Test Screen Grid Aperture Diameters

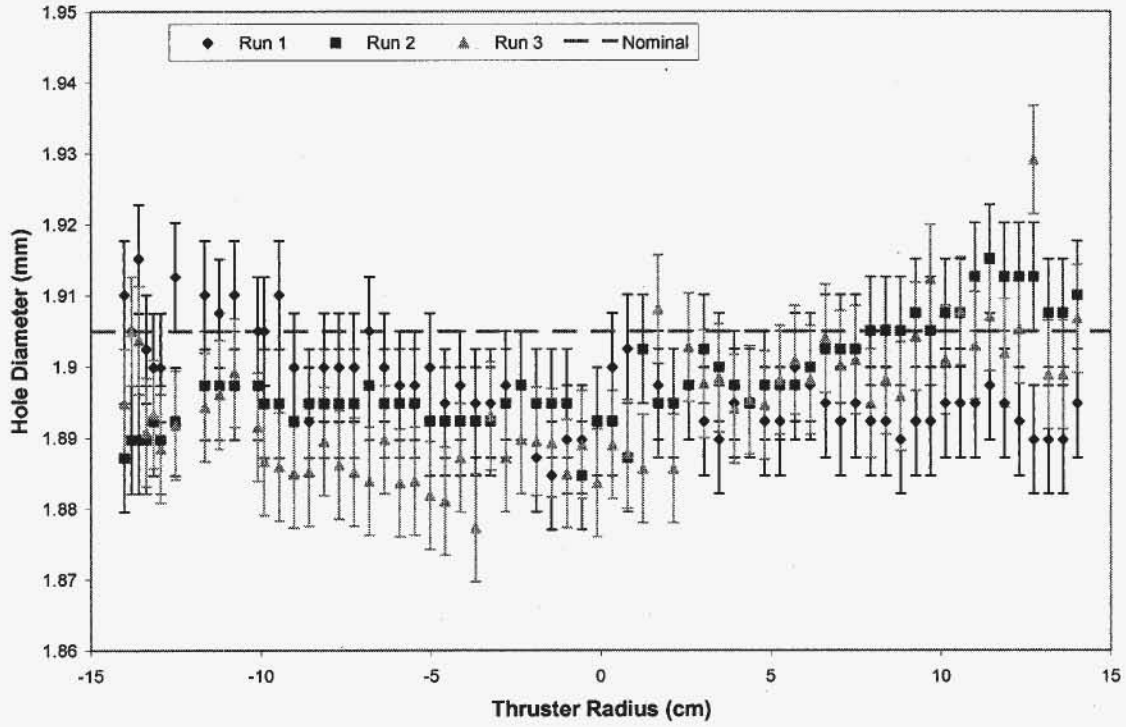


Figure 8. Post-test Screen Grid Aperture Diameter

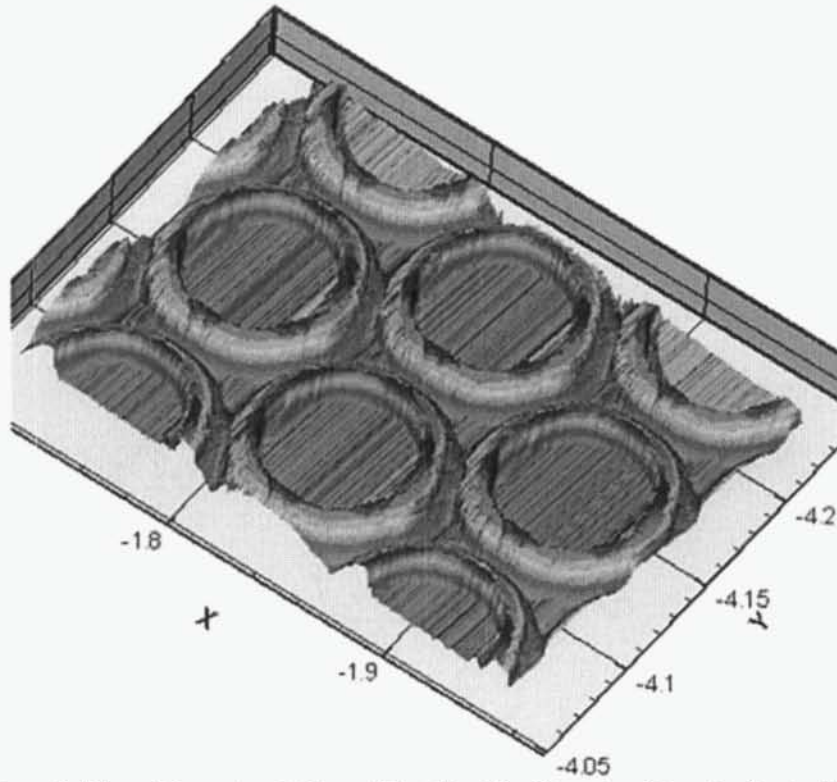


Figure 9. Three-Dimensional View of Post-Test Profilometry Near the Center Hole

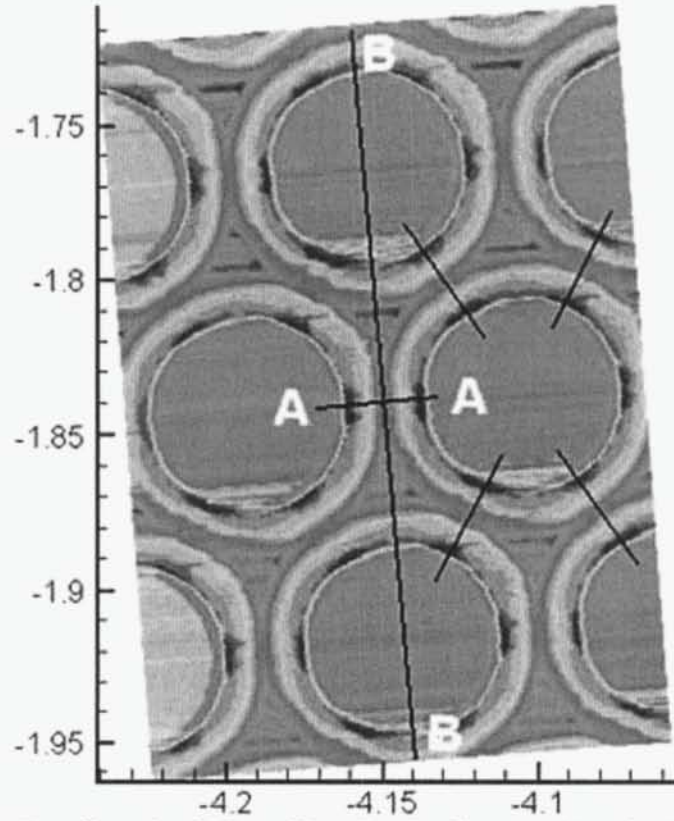


Figure 10. Two-dimensional View of Post-Test Profilometry Near the Center Hole

Center Pits and Grooves Cross-Section

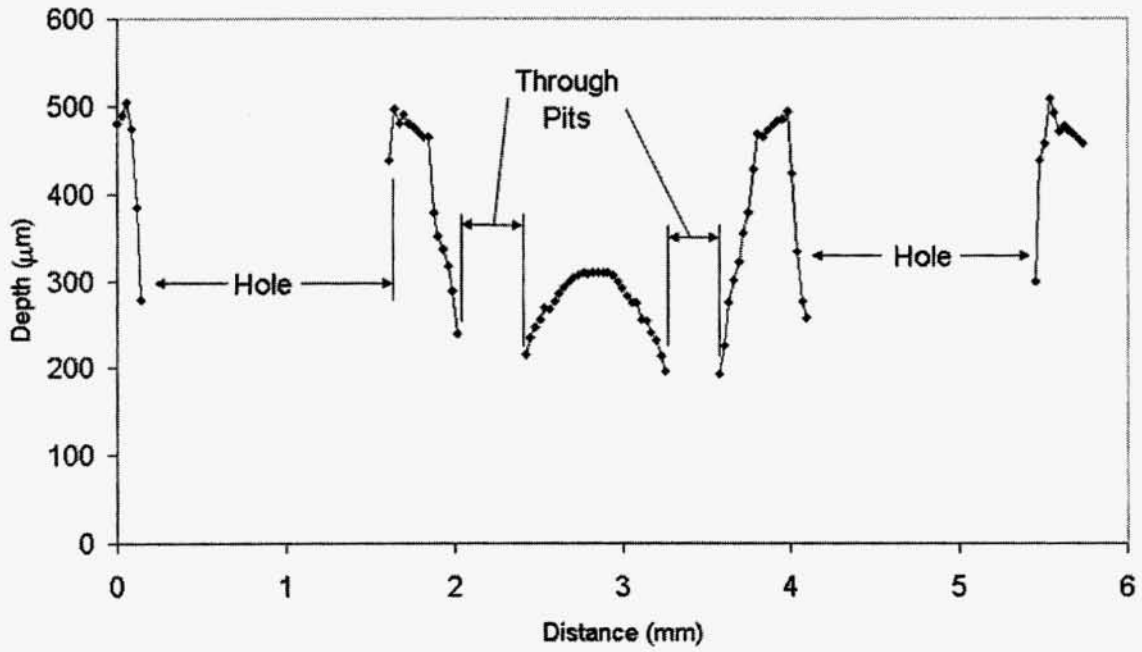


Figure 11. Cross-Section Through Pits and Grooves Pattern of Profilometry Data Near Center Hole

Center Bridge Cross-Section

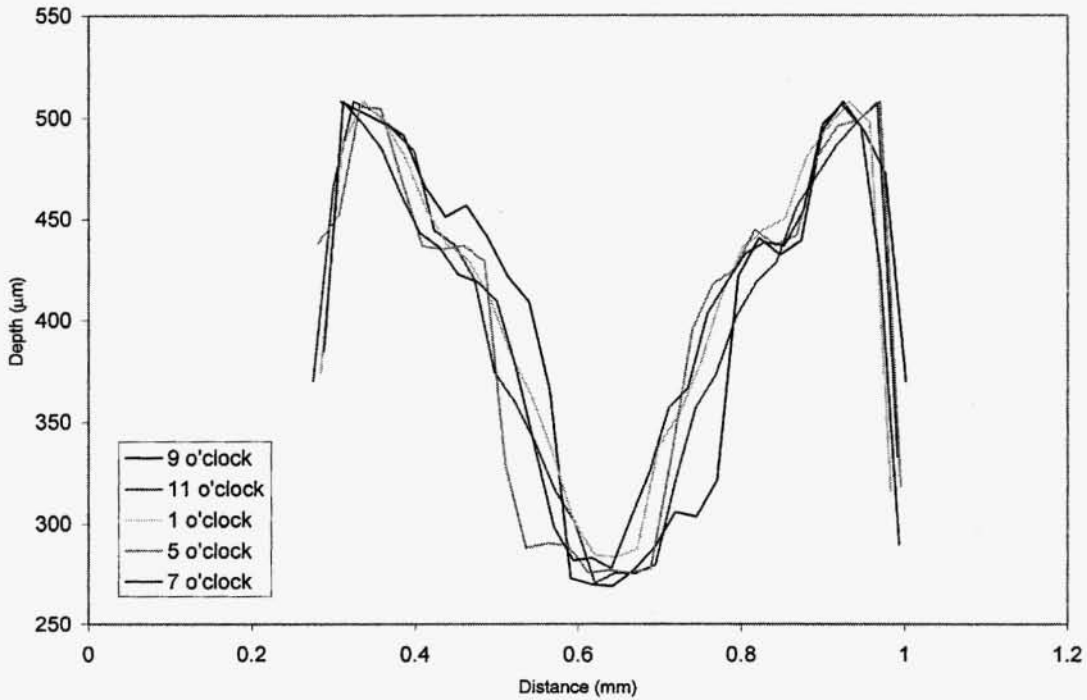


Figure 12. Cross-Sections Through Grooves and Center Hole



Figure 13. Accelerator Grid Upstream Side Undercutting at Through Pit

Pits and Grooves Cross-Sections

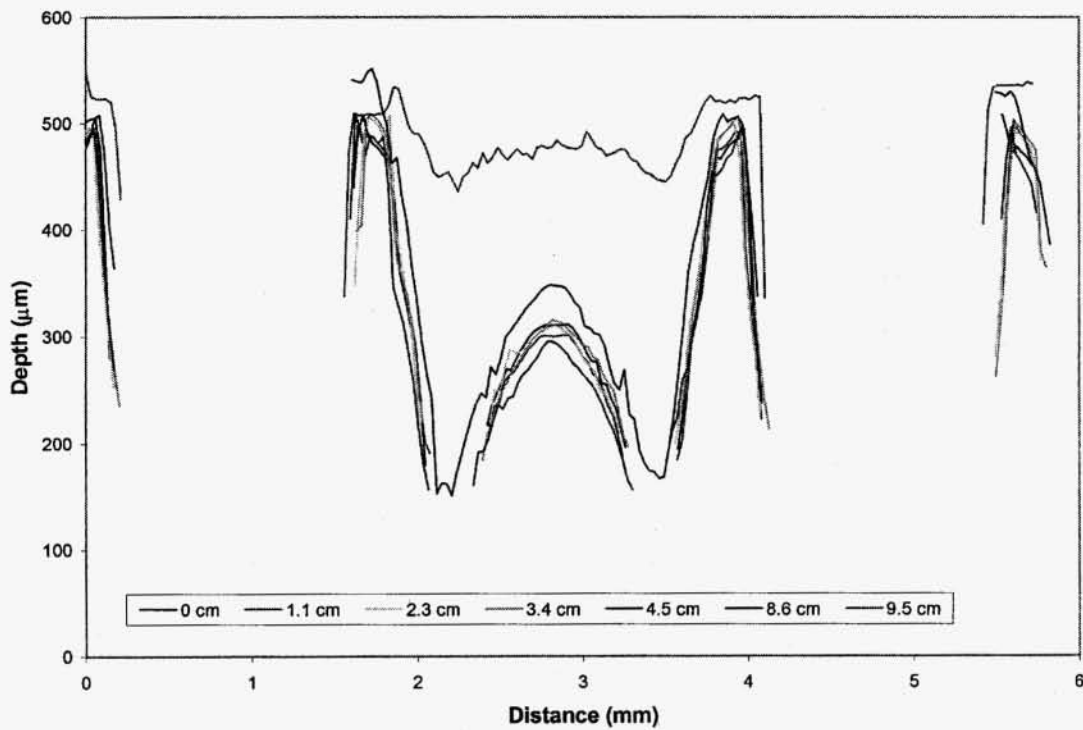


Figure 14. Pits and Grooves Cross-Sections to 9.5 cm Thruster Radius

Post Test Mass Loss Per Hole in Pits and Grooves Pattern

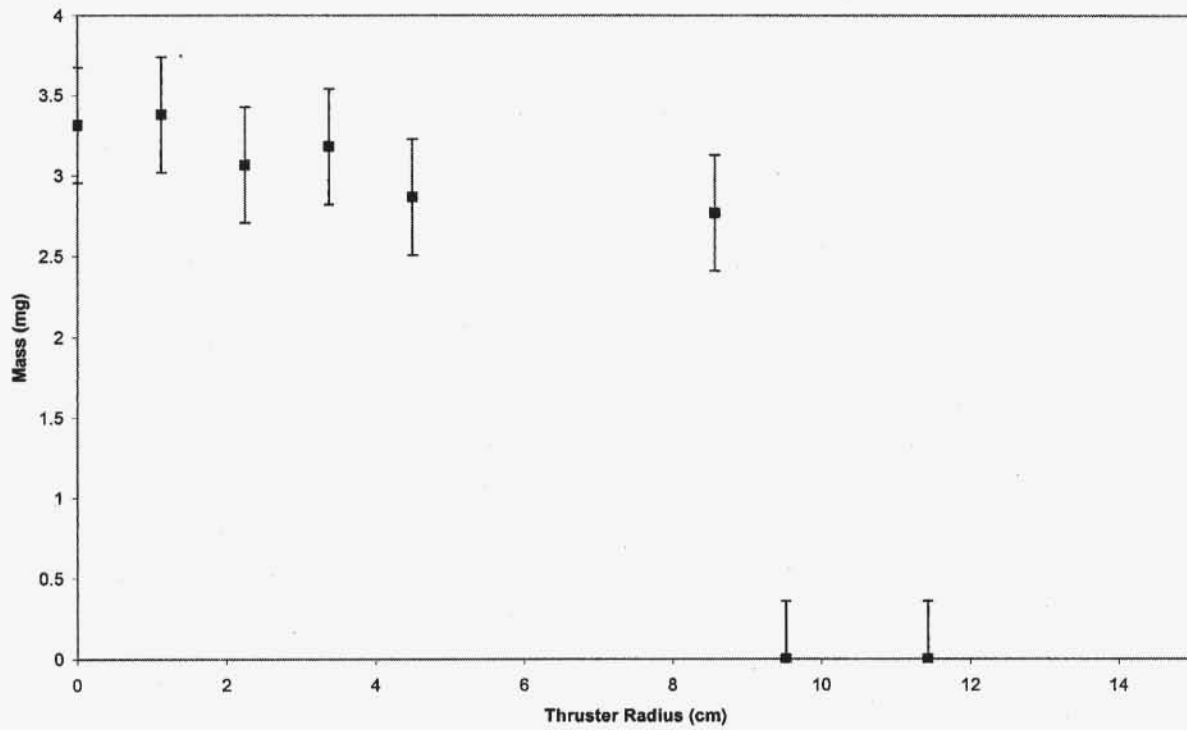


Figure 15. Mass loss in pits and grooves pattern

Post-Test Accelerator Grid Aperture Diameters

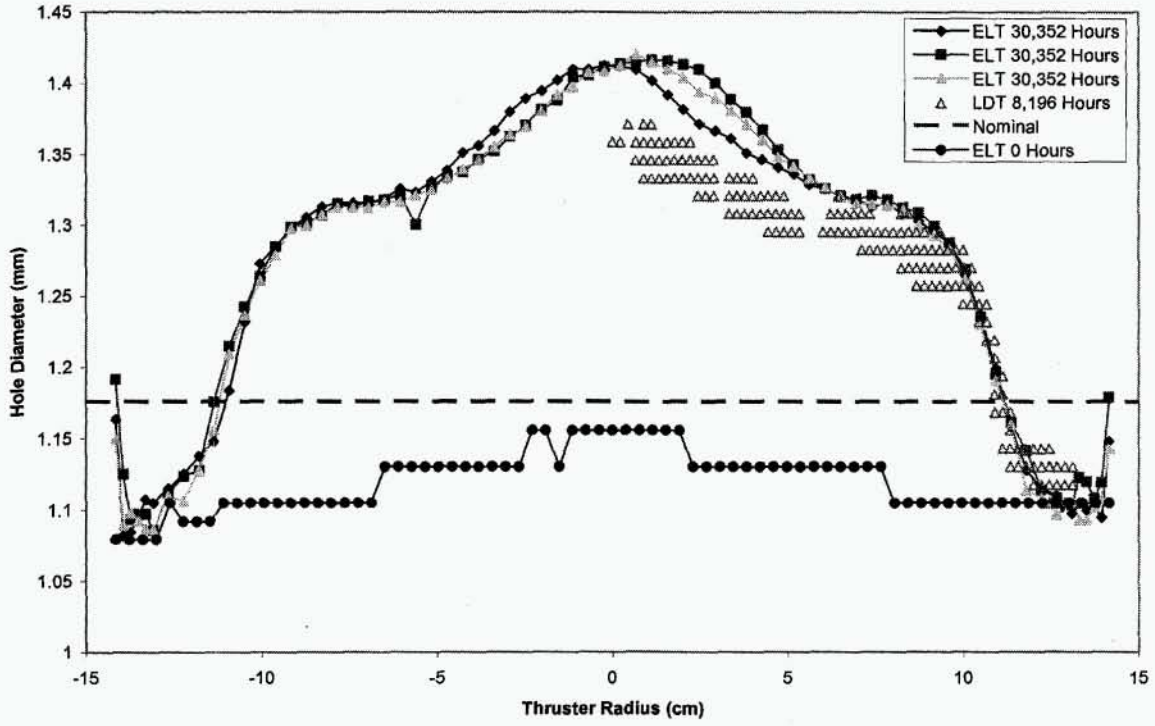


Figure 16. Post-Test Accelerator Grid Aperture Diameters

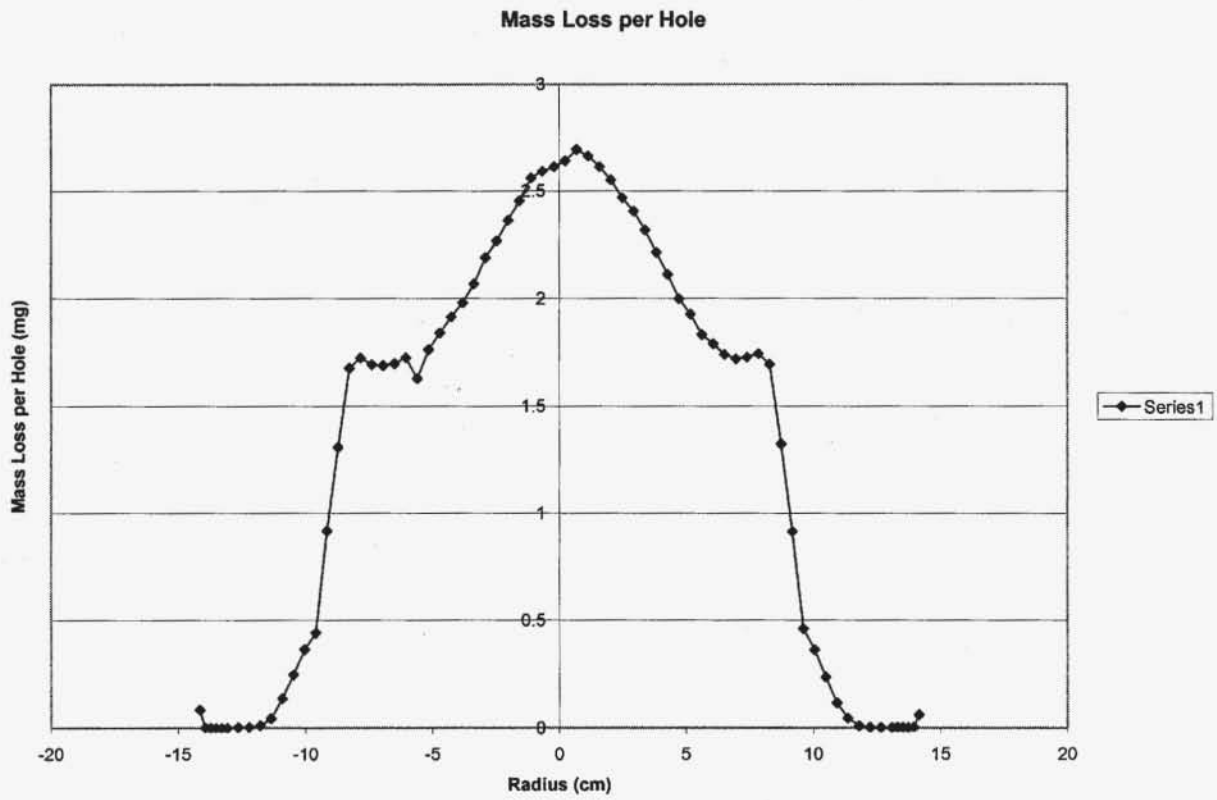


Figure 17. Estimated Mass Loss per Hole due to Aperture Wall Erosion

DS1 Spare Flight Thruster Accelerator Grid Erosion

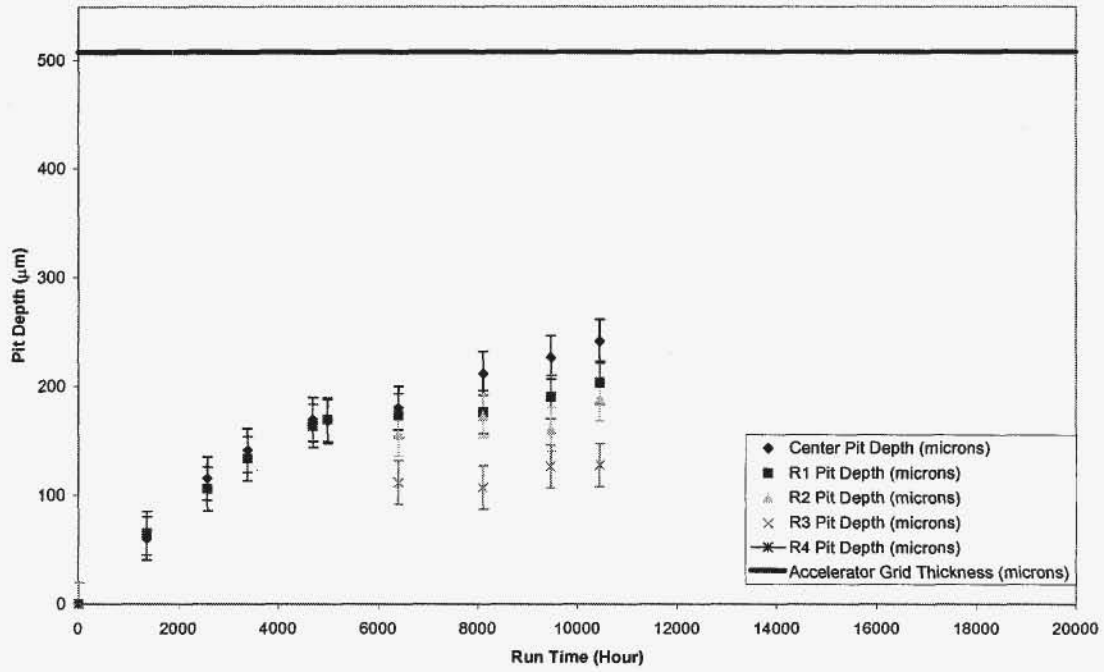


Figure 18. ELT Pit Depth Data

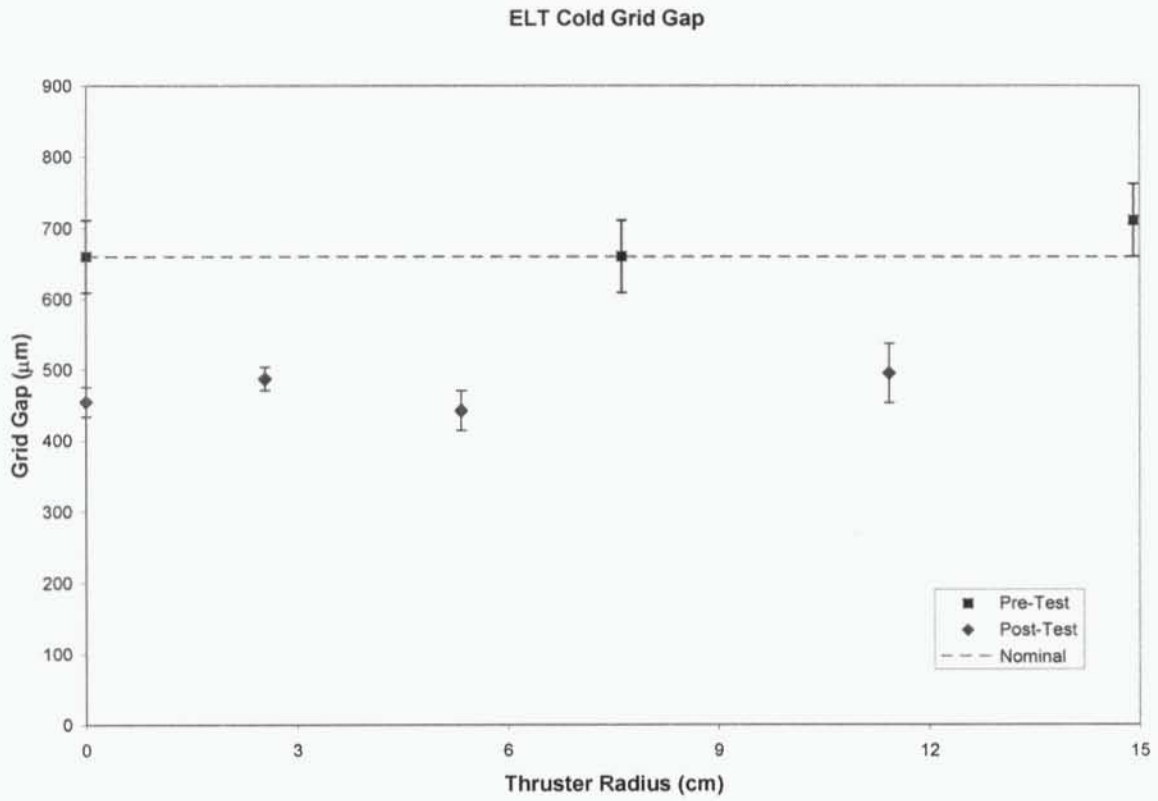


Figure 19. ELT Cold Grid Gap Change

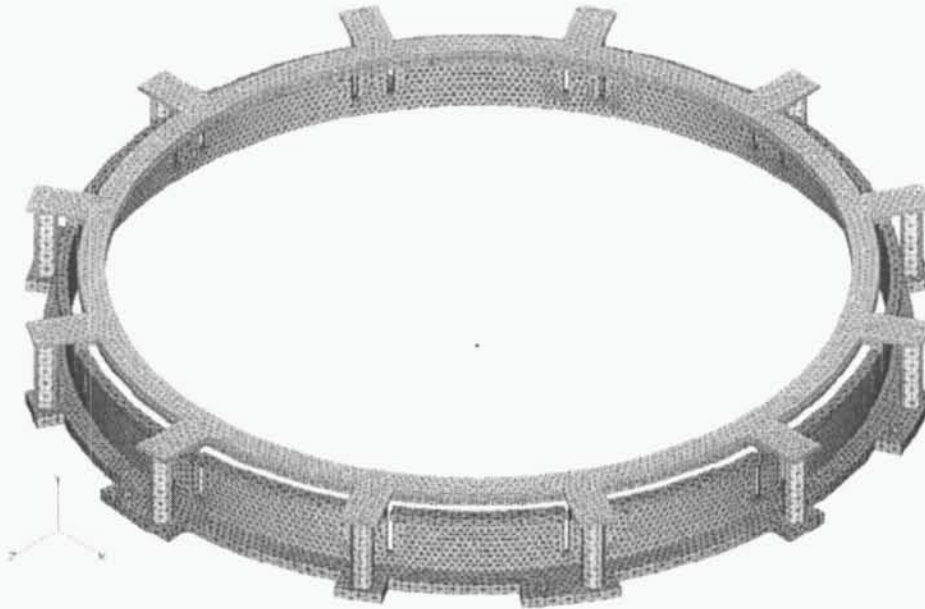


Figure 20. ELT Optics Assembly Model Used in Structural Analysis of Accelerator Grid Stiffening Ring



Accelerator Ring, FEA Results, Stress Relief Load

Figure 21. Computed Residual Stress Load (Von Mises Stress) of the Accelerator Grid Stiffening Ring

End of File

